Evaluating Cell Temperature Models and the Effect of Wind Speed in PV System Capacity Testing

Preprint

Kevin Anderson, Johan Kemnitz, and Matthew Boyd

1 National Renewable Energy Laboratory
2 Signum Energy Analytics

Presented at the 48th IEEE Photovoltaic Specialists Conference (PVSC 48)
June 20-25, 2021

NREL is a national laboratory of the U.S. Department of Energy
Office of Energy Efficiency & Renewable Energy
Operated by the Alliance for Sustainable Energy, LLC

This report is available at no cost from the National Renewable Energy Laboratory (NREL) at www.nrel.gov/publications.

Contract No. DE-AC36-08GO28308

Conference Paper
NREL/CP-5K00-78950
September 2021

Evaluating Cell Temperature Models and the Effect of Wind Speed in PV System Capacity Testing

Preprint

Kevin Anderson, Johan Kemnitz, and Matthew Boyd

1 National Renewable Energy Laboratory
2 Signum Energy Analytics

Suggested Citation
Anderson, Kevin, Johan Kemnitz, and Matthew Boyd. 2021. *Evaluating Cell Temperature Models and the Effect of Wind Speed in PV System Capacity Testing: Preprint*. Golden, CO: National Renewable Energy Laboratory. NREL/CP-5K00-78950. https://www.nrel.gov/docs/fy21osti/78950.pdf.

NREL is a national laboratory of the U.S. Department of Energy
Office of Energy Efficiency & Renewable Energy
Operated by the Alliance for Sustainable Energy, LLC

This report is available at no cost from the National Renewable Energy Laboratory (NREL) at www.nrel.gov/publications.

Contract No. DE-AC36-08GO28308

Conference Paper
NREL/CP-5K00-78950
September 2021

National Renewable Energy Laboratory
15013 Denver West Parkway
Golden, CO 80401
303-275-3000 • www.nrel.gov

NOTICE

This work was authored in part by the National Renewable Energy Laboratory, operated by Alliance for Sustainable Energy, LLC, for the U.S. Department of Energy (DOE) under Contract No. DE-AC36-08GO28308. Funding provided by the U.S. Department of Energy's Office of Energy Efficiency and Renewable Energy (EERE) under Solar Energy Technologies Office (SETO) Agreement Numbers 34348. The views expressed herein do not necessarily represent the views of the DOE or the U.S. Government. The U.S. Government retains and the publisher, by accepting the article for publication, acknowledges that the U.S. Government retains a nonexclusive, paid-up, irrevocable, worldwide license to publish or reproduce the published form of this work, or allow others to do so, for U.S. Government purposes.

Cover Photos by Dennis Schroeder: (clockwise, left to right) NREL 51934, NREL 45897, NREL 42160, NREL 45891, NREL 48097, NREL 46526.

Evaluating cell temperature models and the effect of wind speed in PV system capacity testing

Kevin Anderson[1], Johan Kemnitz[2], Matthew Boyd[1]
[1] NREL, Golden, CO, USA
[2] Signum Energy Analytics LLC, Durham, NC, USA

***Abstract*—Capacity testing is a routine procedure for assessing a photovoltaic system's performance relative to expectations. The most common test method involves fitting a regression model that predicts system output power using operating weather conditions including wind speed. Structural modifications to the regression model to incorporate wind in different ways improved the model's ability to fit measured system performance, but the observed improvements were small and unlikely to change the result of a capacity test. However, the results showed that the choice of reporting wind speed and inclusion or exclusion of wind speed in the performance model used as the test benchmark can significantly change the test result.**

***Index Terms*—photovoltaic, capacity testing, cell temperature, wind speed, ASTM 2848, ASTM 2939**

I. Introduction

Capacity tests are routinely used to evaluate photovoltaic (PV) system performance relative to expectations. Passing a capacity test is a common construction milestone for new PV systems going through acceptance testing and often carries significant financial weight. The wide industry acceptance of capacity tests has been supported by the standardization of testing procedures through ASTM E2848-13 [1] and IEC TS 61724-2 [2]. The ASTM standard is the focus of this paper, as in the authors' experience it is currently the more widely-used of the two standards.

The ASTM E2848-13 standard is centered around a particular multiple linear regression equation that models the relationship between system operating conditions (incident in-plane irradiance G, ambient temperature T_a, and wind speed v) and the corresponding system power output. The regression model has the form

$$P = G \cdot (a + b \cdot G + c \cdot T_a + d \cdot v) \tag{1}$$

where a, b, c, and d are system-specific constants intended to capture the relevant system performance characteristics. Although it may be surprising that a PV system's performance can be adequately captured with only four coefficients, this multiple-linear model is sufficiently robust in practice to enjoy wide use in industry acceptance tests, provided sufficient care is used in data selection. Two sets of coefficients are found by fitting (1) to measured and modeled data sets and then used to calculate measured and expected capacities at a set of reference weather conditions called the reporting conditions [3].

The model form of (1) was used as far back as the late 1980s by the PVUSA project [4]–[7]. This model form has two desirable properties: first, its linear structure is straightforward to fit with basic data analysis software; and second, the model can to some extent be intuited from basic principles, lending some physical interpretability to the model coefficients. However, an aspect of the model that is not as firmly rooted in physics-based reasoning is its implicit cell temperature model. In this paper we investigate alternatives to (1) that account for wind speed's influence on cell temperature in different ways and investigate the effect on fitting ability in a capacity testing context. We also investigate the choice of test reporting conditions on the capacity test result.

The rest of this paper is organized as follows. Section II presents some theory behind the ASTM E2848 regression equation. Section III describes the cell temperature models considered in this work. Section IV describes various aspects of the fitting and test procedure. The fitting and capacity test results are presented in Section V and discussed in Section VI.

II. Regression Model Structure

Theoretical justification of (1) is briefly discussed in [4]–[7]. Here we provide a more detailed mathematical treatment to identify and motivate possible improvements. We start by assuming that a PV system's current I and voltage V at the array's maximum power point are functions of in-plane irradiance G and cell temperature T, and thus so is their product, power P:

$$I = I(G,T) \tag{2}$$
$$V = V(G,T) \tag{3}$$
$$P = P(G,T) = I(G,T) \cdot V(G,T) \tag{4}$$

If the output power P_{stc} at standard conditions $G_{stc} = 1000\,\mathrm{W/m^2}$, $T_{stc} = 25\,^{\circ}\mathrm{C}$ is known, then

$$P_{stc} = P(G_{stc}, T_{stc}) = I(G_{stc}, T_{stc}) \cdot V(G_{stc}, T_{stc}) \tag{5}$$

Taking the first-order Taylor expansions of V and I around (G_{stc}, T_{stc}) gives the approximations:

$$I(G,T) \approx I_{stc} + (G - G_{stc})\frac{\partial I}{\partial G} + (T - T_{stc})\frac{\partial I}{\partial T} \tag{6}$$
$$V(G,T) \approx V_{stc} + (G - G_{stc})\frac{\partial V}{\partial G} + (T - T_{stc})\frac{\partial V}{\partial T} \tag{7}$$

Note that the partial derivative terms are implicitly evaluated at STC. Further approximations allow us to eliminate certain terms in (6) and (7): first, current is proportional to irradiance (i.e., $\partial I/\partial G = I_{stc}/G_{stc}$ and $\partial I/\partial T = 0$); second, voltage does not change with irradiance (i.e., $\partial V/\partial G = 0$). With these approximations, (6) and (7) become:

$$I(G,T) \approx I_{stc} + \frac{I_{stc}}{G_{stc}}(G - G_{stc}) = I_{stc}\frac{G}{G_{stc}} \tag{8}$$

$$V(G,T) \approx V_{stc} + \frac{\partial V}{\partial T}(T - T_{stc}) \tag{9}$$

From $\partial I/\partial T = 0$ it follows that $\partial P/\partial T = I_{stc}\partial V/\partial T$ (again evaluating the partial derivatives at STC). So:

$$V(G,T) \approx V_{stc} + \frac{1}{I_{stc}}\frac{\partial P}{\partial T}(T - T_{stc}) \tag{10}$$

$$= V_{stc}\left[1 + \frac{1}{P_{stc}}\frac{\partial P}{\partial T}(T - T_{stc})\right] \tag{11}$$

Now, multiply I and V to get P:

$$P(G,T) \approx P_{stc}\frac{G}{G_{stc}}\left[1 + \frac{1}{P_{stc}}\frac{\partial P}{\partial T}(T - T_{stc})\right] \tag{12}$$

Recognizing that $P_{stc}^{-1}\partial P/\partial T$ is the module's normalized temperature coefficient of power, the PVWatts DC model [8] emerges. Combining constants and simplifying, we arrive at the general form of our model

$$P(G,T) \approx G(a_0 + a_1 T) \tag{13}$$

where the constants a_0 and a_1 are combinations of basic system parameters:

$$a_0 = \frac{P_{stc}}{G_{stc}} \tag{14}$$

$$a_1 = \frac{1}{P_{stc}}\frac{\partial P}{\partial T}\frac{P_{stc}}{G_{stc}} \tag{15}$$

At this point we are free to choose a model for cell temperature T. For example, we can model T as the linear combination of in-plane irradiance G, ambient temperature T_a, and wind speed v, which reconstructs (1):

$$\begin{aligned} T(G,T_a,v) &= T_a + a'G + d'v \\ \rightarrow P &\approx G(a + bG + cT_a + dv) \end{aligned} \tag{16}$$

Although this linear cell temperature model is straightforward, it seems plausible that replacing it with a physics-based or empirical heat loss model that is nonlinear in wind speed could improve the overall model's predictions. For example, we could choose the Faiman model [9]:

$$T = T_a + \frac{G}{U_0 + U_1 v}, \tag{17}$$

resulting in a modified equation (with constants b_i):

$$P \approx G\left(b_0 + b_1 T_a + \frac{G}{b_2 + b_3 v}\right) \tag{18}$$

The linear combination model and the Faiman model are both fairly simple, using only two constants to capture a system's thermal characteristics. In principle we could use a more complex model like the Fuentes heat transfer model, which takes seven or eight parameters besides the weather inputs, but there is motivation to keep dimension count low to avoid issues when fitting the model.

The above exposition reveals several approximations used to arrive at the standard ASTM 2848 regression model. In this work we focus on the modeled relationship between wind speed and cell temperature, but the other model characteristics may be worth future investigation.

III. Cell Temperature Models

The temperature models considered in this work were chosen based on their popularity in the PV modeling community and their relative simplicity, which is desirable for robust fitting. They also share a basic structure; the models all reduce to a common form if their wind speed coefficients are set to zero. The difference is in how the wind speed term is incorporated. Additionally, they are all implemented in the open-source PV modeling package pvlib-python [10] version 0.8.1 [11].

A. Faiman/PVsyst model

The Faiman model [9] is an empirical heat loss model that has been adopted into IEC standards. The model is as follows:

$$T_{faiman} = T_a + \frac{G}{U_0 + U_1 \cdot v} \tag{19}$$

The PVsyst cell temperature model [12] has a similar structure with additional efficiency and absorption parameters:

$$T_{pvsyst} = T_a + \frac{\alpha(1 - \eta_m)G}{U_c + U_v \cdot v} \tag{20}$$

Noting that the PVsyst coefficients can be combined to reconstruct the Faiman model, the two models are therefore equivalent for regression and treated as a single model hereafter. For more information see Section IV-B2.

B. Sandia (King) model

The Sandia temperature model is part of the broader Sandia Array Performance Model [13]. The cell temperature model takes three non-weather parameters a, b, and ΔT:

$$T_{sandia} = T_a + G\exp(a + b \cdot v) + \frac{G}{1000}\Delta T \tag{21}$$

Because of issues performing fits with this model form, we instead use the module temperature equation:

$$T_{sandia} = T_a + G\exp(a + b \cdot v) \tag{22}$$

This decision is discussed in detail in Section IV-B2. Additionally, because the Sandia model has recommended

TABLE I
NIST GROUND ARRAY METADATA

Coordinates	(39.1319, -77.2141)
PV Module	Sharp NU-U235F2
Array Tilt	20°
Array Azimuth	180°
Rated Capacity	271 $\mathrm{kW_{dc}}$ / 260 $\mathrm{kW_{ac}}$
Data Period	2017-01-01 – 2018-12-31

TABLE II
NREL BEST ROW 9 METADATA

Coordinates	(39.7398, -105.1727)
PV Module	Sunpreme Inc. SNPM-HxB-400
Bifaciality Factor	0.87
Ground Coverage Ratio	0.35
Rated Capacity	7.701 $\mathrm{kW_{dc}}$
Data Period	2019-06-01 – 2020-12-31

coefficient values in wide use in the literature, we also consider a variant called "Sandia (Default)" that fixes the a and b coefficients, leaving only the general a_0 and a_1 parameters free for fitting. Those coefficients are set to the "open rack, glass/polymer" values for the NIST array and "open rack, glass/glass" values for the BEST array (see Table III).

C. Ross model

The Ross cell temperature model [14] takes only one non-weather parameter, the nominal operating cell temperature (NOCT) of the module:

$$T_{ross} = T_a + \frac{\mathrm{NOCT} - 20}{80} G \tag{23}$$

Note that, unlike the previous models, the Ross model does not explicitly consider wind speed. Note also that, in its standard form, the expected units for G are different from the other models. For the purposes of this work the equation was adjusted to have units consistent with those of the other models.

D. ASTM (linear) model

As a basis for comparison, the final model considered here is the cell temperature model implicit in (1), with two effective parameters:

$$T_{astm} = T_a + bG + cv \tag{24}$$

It should be pointed out that (24) is not typically used as a standalone model, but we treat it as such here for consistency with (13).

IV. METHODOLOGY

Combining the above models with (13), we use the open-source python package SciPy v1.3.1 [15] to perform nonlinear least-squares fits to two public PV data sets. The first is from the National Institute of Standards and Technology (NIST) [16]. We use data from the NIST ground array, a fixed-tilt array with monofacial modules. The second is from row 9 of the Bifacial Experimental Single-axis Tracking (BEST) array from the National Renewable Energy Laboratory (NREL) [17]. The full data sets are divided into 14 day test intervals. System configuration details are listed in Tables I and II.

Note that because the BEST array has bifacial modules, we follow the approach in [18] and compute total in-plane irradiance considering irradiance on both the front- (G_f) and rear-side (G_r) surfaces:

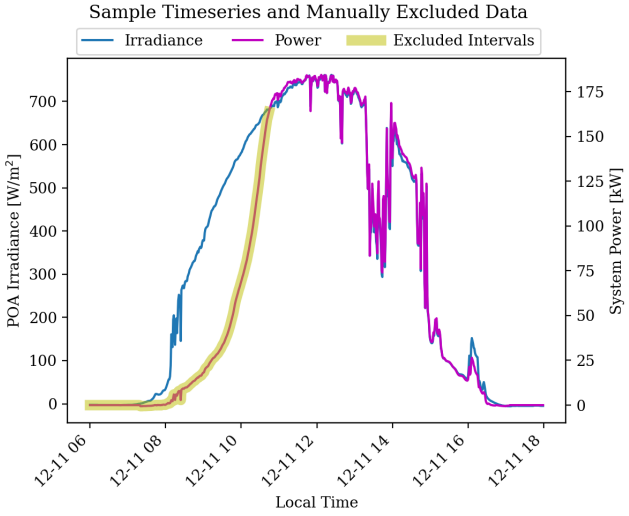

Fig. 1. Sample time series data from NIST, 2017-12-11 highlighting intervals removed due to partial snow cover on the array that later melted.

$$G = G_f + \varphi G_r \tag{25}$$

where φ is the module's bifaciality factor. This combined irradiance quantity takes the place of G when performing model fits.

A. Data Filtering

As is typical in ASTM-style capacity testing, the data are first filtered for linearity, removing data according to the following criteria:

- 1-min samples within 98% of the maximum power when the PV system inverter may be power-limited (clipping)
- Data with non-clear conditions using the Reno & Hansen clear-sky detection algorithm implemented in [11]
- Data with 15-minute average in-plane irradiance below 400 $\mathrm{W/m^2}$
- Data with 15-minute average power below 50 $\mathrm{kW_{ac}}$ (NIST) or 0.1 $\mathrm{kW_{dc}}$ (BEST)
- Data affected by shading or snow cover on the array. Fig. 1 shows an example exclusion.

B. Least-Squares Fitting

Fitting the models to the measured data presented certain challenges, as described below.

TABLE III
INITIAL PARAMETER VALUES

Model	Parameter	Initial Value	Units
Faiman	U_0	25	$(\mathrm{W/m^2})\,^\circ\mathrm{C}^{-1}$
Faiman	U_1	6.84	$(\mathrm{W/m^2})\,^\circ\mathrm{C}^{-1}\,(\mathrm{m/s})^{-1}$
Sandia	a	$-3.56/-3.47$	unitless
Sandia	b	$-0.075/-0.0594$	$(\mathrm{m/s})^{-1}$
Ross	NOCT	40	$^\circ\mathrm{C}$
ASTM	b	1	$(\mathrm{W/m^2})^{-1}\,^\circ\mathrm{C}$
ASTM	c	1	$(\mathrm{m/s})^{-1}\,^\circ\mathrm{C}$

1) Initial Values: Unlike ordinary linear least-squares fitting, nonlinear least-squares fitting generally cannot employ a closed-form expression for the fitted parameter values. The approach is instead to use numerical optimization techniques like the Levenberg-Marquardt algorithm, as used here, that converge to a local error minimum in the parameter space. Because nonlinear functions can have multiple local minima, a successful convergence does not guarantee that the intended minimum was found. To guide the optimizer towards minima of interest, the initial parameter values are set to suggested parameter values found in the literature. In the case of the linear cell temperature model, initial values were set to 1. Table III lists the set of initial values for each model. Note that the starting values for the Sandia model are different for the two arrays based on module construction (glass/polymer vs glass/glass) and shown as NIST/BEST, respectively.

2) Redundant Parameters: As briefly mentioned when discussing the Faiman and PVsyst models, redundant parameters should be combined prior to fitting the model. As an example, take the PVsyst model (20). The α and η_m parameters are redundant because any change in one can be exactly canceled by the other. When a model has redundant parameters, the local error minima in the parameter space become infinite sets of points instead of single points, meaning the optimizer might converge to any point in the set and still have found a minimum. To illustrate the concept, consider fitting the PVsyst model to a hypothetical data set where the optimizer converges to parameter values $\alpha = \eta_m = 0.5$. Referring back to (20), those parameter values will yield identical predictions to an alternative set of values $\alpha = 1$ and $\eta_m = 0.75$. Because the model predictions are identical, the optimizer will have no preference between the two and may select either. And in fact it may select any pair of values satisfying the relation $\alpha(1-\eta_m) = K$, where in this example $K = 0.25$. That set of pairs forms a line in the $\alpha - \eta_m$ plane. Therefore, to restrict the parameter space to contain unique minima, it is desirable to combine redundant parameters, as we've done with the Faiman and PVsyst models.

To take it a step further, a similar redundancy exists between the a and ΔT parameters in (21). This can be shown analytically with the Maclaurin expansion of the exponential function or graphically as in Fig. 2. To eliminate the redundancy, we drop the ΔT term, reducing the Sandia cell temperature model (21) to the Sandia module temperature model (22).

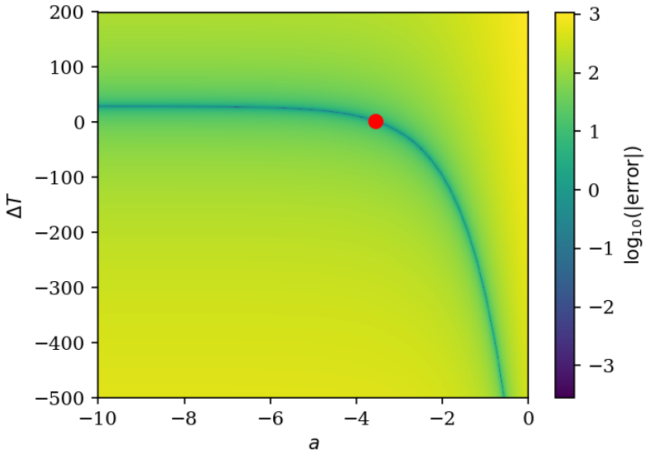

Fig. 2. Error surface for the $a - \Delta T$ plane at $b = -0.075$ in the parameter space of the Sandia cell temperature model. The redundancy between a and ΔT creates a family of minima in the error surface (dark curve). Error is calculated assuming parameter values $a = -3.56$, $b = -0.075$, and $\Delta T = 3$ (marked with the red circle) and weather conditions $G = 1000$, $T_a = 20$, and $v = 1$.

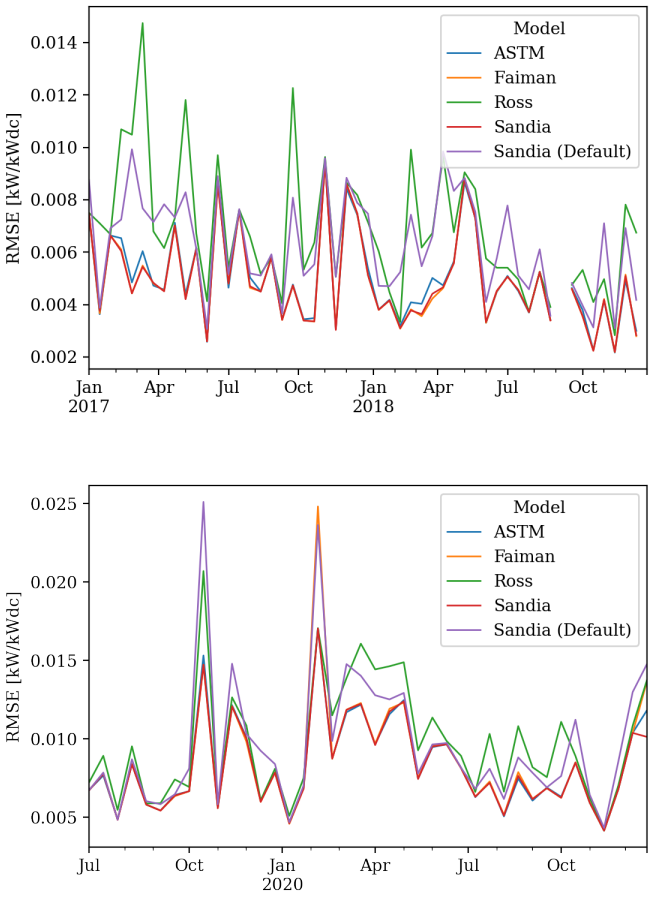

Fig. 3. RMSE for each test interval for the NIST (upper) and BEST (lower) arrays. The more constrained models (Ross, Sandia Default) generally show higher error than the more general models (ASTM, Faiman, Sandia), which all show about the same error. Missing intervals are due to insufficient data after filtering. RMSEs are shown as a fraction of system DC capacity.

C. Model Comparison

After performing the fits, the goodness of fit is evaluated by calculating the root-mean-squared error (RMSE) for each test interval and each model. However, although fit statistics like RMSE are useful determining if one model's fit is better than another in an absolute sense, they do not provide a straightforward indication of whether that fit improvement is large enough to be meaningful in real-world contexts. To evaluate the relative performance of our alternate regression models in a capacity testing context, we perform capacity tests using each model in turn and compare the test results. With the exception of the modifications to the regression equation, the test procedure follows the ASTM E2848-13 standard. A PVsyst model was built for each of the two systems and used as the reference performance in the capacity test iterations. Note that a reference PVsyst PAN file for the BEST modules was not available. Instead, the PAN file for a bifacial Mono-PERC module of similar wattage was used. As the NIST Ground-Mount Array has been in operation since 2012, a cumulative degradation of -2.8% was applied to the model. No further reductions for degradation were applied beyond this initial assumption.

V. Results

A. Fit Results

Figs. 3 shows RMSE for each test interval and each model for the NIST and BEST arrays. Although the Faiman and Sandia models do achieve lower error than the base ASTM model in some intervals, the improvement is modest, especially compared with the difference between ASTM and Ross.

Fig. 4 shows the combined fit residuals for the Ross model across all test intervals for the NIST array. The grey lines show the Theil-Sen trend for each test interval, generally indicating positive residual trends with increasing wind speed.

B. Capacity Test Results

Fig. 5 shows the final capacity ratios for the NIST and BEST arrays, respectively, for each model and test interval. In both cases the final test results for the ASTM, Faiman, and Sandia models are nearly identical. However, the results for the Ross model and the Sandia model with default parameters show a positive shift. This shift is investigated further in Section V-C.

The downward spikes in October 2019 and February 2020 in Fig. 5 for the BEST array are likely due to a combination of high ground albedo during those test intervals and optimistic assumption of rearside efficiency; assuming a lower bifaciality factor to account for additional rearside effects like mismatch and racking shading brought results back in line with the other test intervals.

Although describing system performance is not a goal of this work, Fig. 5 shows two trends worth mentioning. First, the NIST array shows a marked performance decrease at the end of 2018, but we did not investigate why this may be. Second, the BEST array shows a general trend of performance decline that may be explained by nonlinear degradation reported for silicon heterojunction modules [19], although the rate of decline seen here is perhaps faster than expected.

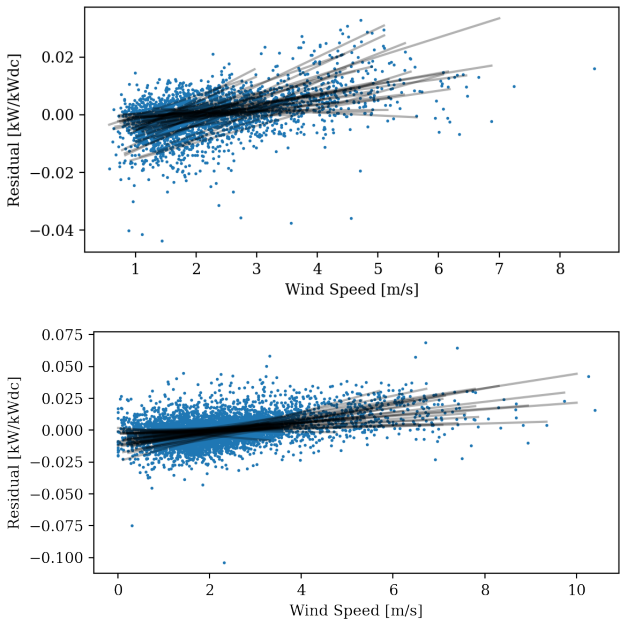

Fig. 4. NIST (top) and BEST (bottom) fit residuals (blue dots) and Theil-Sen trends (grey lines) for each test interval for the Ross model. Positive trends indicate the Ross overpredicts power at low wind speed and underpredicts power at high wind speed, which is consistent with expectations. Residuals are shown as a fraction of system DC capacity.

C. Inclusion of Wind Speed and Effect of Reporting Conditions

ASTM E2939 [3], a supplement to ASTM E2848 specifying how to find the reporting conditions used for calculating the measured and expected capacity values, uses the average post-filtering wind speed for the reporting condition. However, in the authors' experience, industry tests sometimes assume a reporting wind speed of 1 m/s instead of taking an average value.

PVsyst is commonly used to generate the baseline performance models used in utility-scale capacity testing. However, the wind speed coefficient U_v in its cell temperature model (20) is set to zero by default, and is usually left unchanged by industry analysts, resulting in negligible correlation between modeled power and wind speed. In this case the fitted wind coefficient for the modeled data set will be near zero, resulting in little change in the expected capacity when varying the wind speed component of the reporting conditions. However, Fig. 4 suggests at least a modest effect of wind speed on performance. The PVsyst documentation also mentions a set of alternative coefficients that do consider wind speed. We did not investigate how our results change by using those coefficients, but they may be more appropriate in light of Figs. 4 and 6.

To the extent that wind speed does affect real system performance, the measured wind coefficient will be nonzero and varying the wind speed reporting condition will change the measured capacity. This means that the final capacity test

Fig. 5. Capacity ratios (measured to expected) using each temperature model for the NIST (upper) and BEST (lower) arrays. Tests with mismatched wind response (ASTM, Faiman, Sandia) are offset from tests with matched wind response (Sandia Default, Ross). Missing intervals are due to insufficient data after filtering.

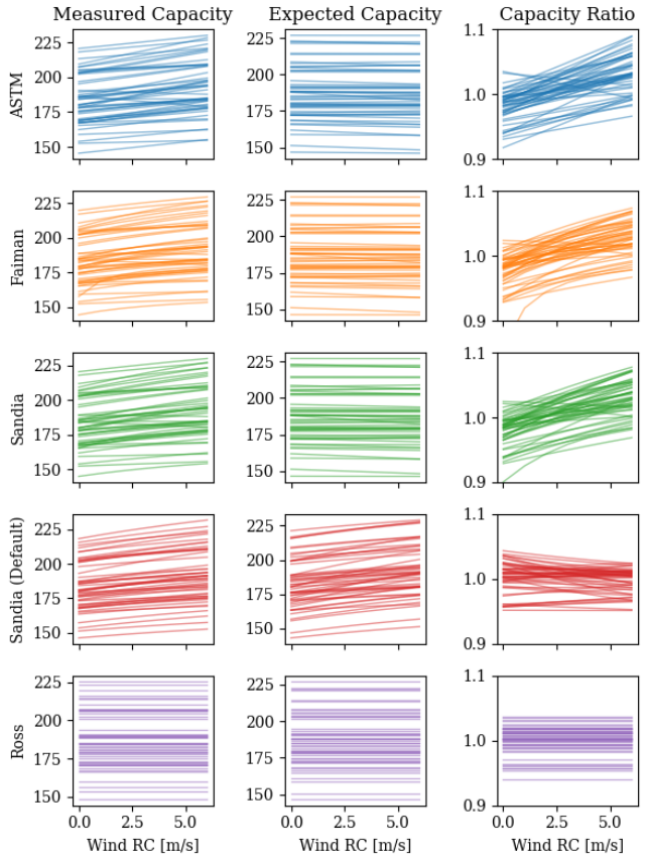

Fig. 6. Measured capacity, expected capacity, and their ratio for each temperature model across all test intervals for the NIST array. Each line represents one test interval. If only one of the capacities is affected by wind speed, the capacity ratio varies significantly with choice of wind speed reporting condition.

result (the ratio of measured to expected capacities) can be influenced by the choice of reporting condition. Fig. 6 shows how the choice of wind speed reporting condition affects the capacity test results for the NIST array. In the cases where a wind speed coefficient is fitted to the model, varying the wind speed reporting condition from 0 to 5 m/s results in a change in test result of over 4 percentage points on average. This variation is rooted in the fact that only one of the capacities (measured or expected) is actually affected by wind speed except for the Sandia-Default model (both capacities are affected by wind) and Ross model (neither capacity is affected by wind). For the latter two models, the capacity test result is more stable across changes in wind speed reporting condition. Fig. 7 shows this difference another way via the distribution of least-squares slopes fitted to each line in the third column of Fig. 6, where the slope is the rate of change in the capacity ratio with changing wind reporting condition. The slope distributions for the first three models are located away from zero while the latter two models are centered around zero (or identically zero in the case of Ross).

Note that the capacity ratios for the BEST array (using the

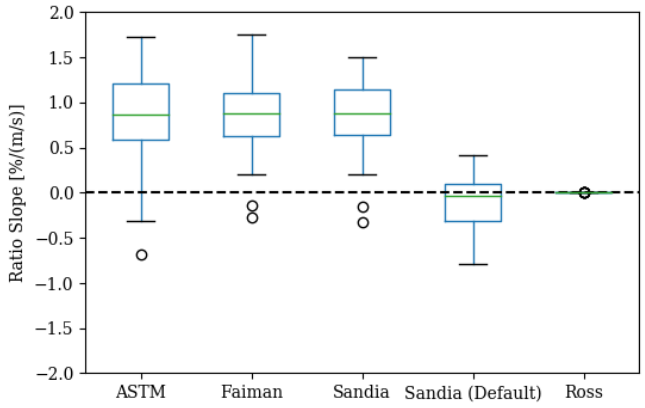

Fig. 7. Distribution of least-squares slopes for each test interval in Fig. 6. The slope is the change in capacity ratio for each increment in wind reporting condition. The first three models are centered around a slope of about 0.8% per wind speed increment, meaning increasing the wind reporting condition by 1 m/s increases the capacity ratio by about 0.8%. The latter two are centered around zero, indicating better stability with changing wind reporting condition.

three wind-sensitive models) also increased when increasing the wind speed reporting condition.

VI. Discussion

The fit statistics and capacity test results shown in Figs. 3 and 5 show little difference between the three wind-sensitive models (ASTM, Faiman, and Sandia), suggesting there is little practical benefit to using a nonlinear wind model in the regression itself.

However, Section V-C reveals an important point: for a capacity test to be stable across changes in reporting wind speed, the performance model's response to wind speed must be similar to the real system's response. By omitting the effect of wind speed on system performance, as is the default in PVsyst, the capacity test is made susceptible to bias based on the reporting wind condition. For the NIST system this bias amounts to several percent across the range of reasonable reporting wind speeds, a difference larger than the margin by which many tests pass or fail. Possible resolutions to this problem include: 1) determining a wind reporting condition that eliminates bias; 2) removing wind speed from the regression so that neither measured nor expected capacity varies with wind speed (as done in the Ross regression); or 3) including the effect of wind speed in the performance model. It is difficult to suggest concrete guidance for implementing option 1 in practice, but options 2 and 3 are easily implemented in a practical capacity test. As seen in Fig. 4 and the broader PV literature, system performance is generally affected by wind, so option 3 may be the best solution. However, the specific choice of coefficients to use in modeling is still an open question and may be the subject of future work.

Acknowledgment

This work was authored in part by Alliance for Sustainable Energy, LLC, the manager and operator of the National Renewable Energy Laboratory for the U.S. Department of Energy (DOE) under Contract No. DE-AC36-08GO28308. Funding provided by the U.S. Department of Energy's Office of Energy Efficiency and Renewable Energy (EERE) under Solar Energy Technologies Office (SETO) Agreement Numbers 34348. The views expressed in the article do not necessarily represent the views of the DOE or the U.S. Government. The U.S. Government retains and the publisher, by accepting the article for publication, acknowledges that the U.S. Government retains a nonexclusive, paid-up, irrevocable, worldwide license to publish or reproduce the published form of this work, or allow others to do so, for U.S. Government purposes.

References

[1] "Test method for reporting photovoltaic non-concentrator system performance," ASTM International, Standard E2848-13, 2013. [Online]. Available: https://doi.org/10.1520/E2848-13

[2] "Photovoltaic system performance - part 2: Capacity evaluation method," IEC, Standard TS 61724-2, 2016.

[3] "Standard practice for determining reporting conditions and expected capacity for photovoltaic non-concentrator systems," ASTM International, Standard E2939-13, 2013. [Online]. Available: https://doi.org/10.1520/D2939-13

[4] C. Jennings, "PV module performance at PG&E," in *Proceedings of the 20th IEEE PV Specialists Conference*, Las Vegas, NV, 1988, p. 1225–1229.

[5] C. J. Weinberg, "PG&E research, development, demonstration, and future options for photovoltaic technology: an overview," in *Proceedings of the 4th International PV Science and Engineering Conference*, Sydney, Australia, 1989, pp. 189–195.

[6] R. Dows and E. Gough, "PVUSA procurement, acceptance, and rating practices for photovoltaic power plants," Tech. Rep., Sep. 1995. [Online]. Available: https://doi.org/10.2172/119944

[7] C. Whitaker, T. Townsend, J. Newmiller, D. King, W. Boyson, J. Kratochvil, D. Collier, and D. Osborn, "Application and validation of a new PV performance characterization method," in *Conference Record of the Twenty Sixth IEEE Photovoltaic Specialists Conference*. IEEE, 1997. [Online]. Available: https://doi.org/10.1109/pvsc.1997.654315

[8] A. P. Dobos, "PVWatts version 5 manual," National Renewable Energy Laboratory, Golden, CO, Tech. Rep. NREL/TP-6A20-62641, 9 2014.

[9] D. Faiman, "Assessing the outdoor operating temperature of photovoltaic modules," *Progress in Photovoltaics: Research and Applications*, vol. 16, no. 4, pp. 307–315, Jun. 2008. [Online]. Available: https://doi.org/10.1002/pip.813

[10] W. Holmgren, C. Hansen, and M. Mikofski, "pvlib python: a python package for modeling solar energy systems," *Journal of Open Source Software*, vol. 3, no. 29, p. 884, 2018. [Online]. Available: https://doi.org/10.21105/joss.00884

[11] W. Holmgren *et al.*, "pvlib/pvlib-python: v0.8.1," Jan. 2021. [Online]. Available: https://doi.org/10.5281/zenodo.4417742

[12] PVsyst, "Array thermal losses," https://www.pvsyst.com/help/thermal_loss.htm, accessed: 2021-01-14.

[13] D. King, W. Boyson, and J. Kratochvill, "Sandia photovoltaic array performance model," Sandia National Laboratories, Albuquerque NM, Tech. Rep. SAND2004-3535, 2004. [Online]. Available: https://prod.sandia.gov/techlib-noauth/access-control.cgi/2004/043535.pdf

[14] R. G. J. Ross, "Design techniques for flat-plate photovoltaic arrays," in *15th IEEE Photovoltaic Specialist Conference*. IEEE, 1981.

[15] P. Virtanen *et al.*, "SciPy 1.0: Fundamental Algorithms for Scientific Computing in Python," *Nature Methods*, vol. 17, pp. 261–272, 2020. [Online]. Available: https://doi.org/10.1038/s41592-019-0686-2

[16] M. Boyd, Tzong Hao Chen , and B. Dougherty, "NIST campus photovoltaic (PV) arrays and weather station data sets," 2017. [Online]. Available: https://doi.org/10.18434/M3S67G

[17] S. Ayala, "BEST field data - data and resources," 2020. [Online]. Available: https://doi.org/10.21948/1787805

[18] M. Waters, C. Deline, J. Kemnitz, and J. Webber, "Suggested modifications for bifacial capacity testing," in *2019 IEEE 46th Photovoltaic Specialists Conference (PVSC)*, vol. 2, 2019, pp. 1–6. [Online]. Available: https://doi.org/10.1109/PVSC40753.2019.9198974

[19] D. C. Jordan, C. Deline, S. Johnston, S. R. Rummel, B. Sekulic, P. Hacke, S. R. Kurtz, K. O. Davis, E. J. Schneller, X. Sun, M. A. Alam, and R. A. Sinton, "Silicon heterojunction system field performance," *IEEE Journal of Photovoltaics*, vol. 8, no. 1, pp. 177–182, Jan. 2018. [Online]. Available: https://doi.org/10.1109/jphotov.2017.2765680